VUV and ultrasoft X-ray diode detectors for Tokamak plasmas

Ping Lee* and J. Gernhardt
Max-Planck-Institut für Plasmaphysik,
EURATOM-Association, 8046 Garching, FRG

C.J. Armontrout
KMS Fusion, Inc.
Ann Arbor, Mi 48106

R.T. Snider
GA Technologies
San Diego, CA 92138

IPP III/128 November 87

MAX-PLANCK-INSTITUT FÜR PLASMAPHYSIK

8046 GARCHING BEI MÜNCHEN

MAX-PLANCK-INSTITUT FÜR PLASMAPHYSIK

GARCHING BEI MÜNCHEN

VUV and ultrasoft X-ray diode detectors for Tokamak plasmas

Ping Lee* and J. Gernhardt
Max-Planck-Institut für Plasmaphysik,
EURATOM-Association, 8046 Garching, FRG

C.J. Armontrout
KMS Fusion, Inc.
Ann Arbor, Mi 48106

R.T. Snider
GA Technologies
San Diego, CA 92138

IPP III/128 November 87

*GA Technologies, San Diego

Die nachstehende Arbeit wurde im Rahmen des Vertrages zwischen dem Max-Planck-Institut für Plasmaphysik und der Europäischen Atomgemeinschaft über die Zusammenarbeit auf dem Gebiete der Plasmaphysik durchgeführt.

VUV and ultrasoft X-ray diode detectors for Tokamak plasmas

Ping Lee* and J. Gernhardt
Max-Planck-Institut für Plasmaphysik,
EURATOM-Association, 8046 Garching, FRG

C.J. Armontrout
KMS Fusion, Inc.
Ann Arbor, Mi 48106

R.T. Snider
GA Technologies
San Diego, CA 92138

ABSTRACT

Ultrasoft X-ray diode (USXRD) arrays have been used on D-IIID and ASDEX to study plasma edge radiation, in the photon energy range from 10eV to 10keV. The detectors are extremely useful and versatile due to their simplicity and compactness. Furthermore, absolute quantum efficiencies (QE) of many photocathodes such as vitreous C, Al, Cu, CuI, CsI and Au have been measured in recent years. With filter technique, broadband resolution, $E/\Delta E \sim 1$, is possible. QE comparison of USXRD with semiconductor XRD is also presented to better understand the regions of applicability for each detector.

1. INTRODUCTION

Solid state X-ray diodes (XRDs) such as pin diodes and surface barrier detectors have become standard tokamak plasma diagnostics /1, 2/. One and two dimensional imaging arrays have provided crucial information for the understanding of the dynamics of internal MHD activities such as sawteeth, magnetic islands, and of radiation losses /1 - 5/. The photon energy response of these detectors are limited in the low energy range by the deadlayer (undepleted portion of the silicon wafer, nominal thickness ~0.5 μm) to about 0.5keV, and in the high energy range by wafer thickness (nominal thickness ~200 μm) to about 10keV. Additionally, a beryllium window or some overcoating is necessary to shield the diodes from visible light, thus further reducing the low energy response. Typical detector energy sensitive range is thus about 3keV to 10keV. Within this energy range, solid state XRDs are well suited as tokamak

diagnostics due to their high quantum effiency (QE = electrons produced/incident photon) and fast time response (~1 μs). For example, the QE ~ 1400 for 5keV photons, assuming the usual 3.5eV per electron-hole pair in silicon.

With increasing awareness of the importance of edge plasma physics such as plasma-wall interactions /6/ and H-mode phenomena /7/, needs now exist for simple broadband detectors with spectral response in the VUV and ultrasoft X-rays region (10eV - 1keV) that can complement the silicon XRDs. However, such broadband detectors with well calibrated QE and submicrosecond temporal responses have not been available on large tokamaks. This region of the electromagnetic spectrum is covered by normal and grazing incidence spectrometers and monochrometers. Due to their complexity and physical bulk, it is difficult to field more than a few on any given machine. Bolometers, on the other hand, can measure the total radiation loss of a plasma with no spectral resolution.

The photoelectric effect has had a wide range of applications in modern instrumentation such as ionization chambers, proportional counters, photomultipliers, and photodiodes to name just a few. One important advantage of the photoelectric process is linearity (better than 1% over 15 orders of magnitude for most metallic photocathodes and modest extraction voltages /8/). The detector of interest in this report is the biplanar ultrasoft X-ray diode (USXRD) which has been extensively used in high fluence pulsed applications such as laser produced plasmas /9/. The important properties of USXRDs are: response in the 10eV to 10keV region, well-known QEs, fast time response (<10 ns, limited by amplifier and digitizer speed), neutron tolerance /10/, simplicity and compactness.

Taylor, et al. /11/ have used tungsten photocathode USXRD arrays on Macrotor to study impurity radiation and disruptions. These arrays were operated without filters with a bias of 15V. The observed photoelectric current was 100 $\mu A/cm^2$, hence easily detectable.

In this communication, we report on the application of multichannel USXRD on D-IIID and ASDEX using filters for broadband energy resolution, $E/\Delta E \sim 1$. Section 2 describes the operating principle, design, QE of USXRD. In section 3, some examples of measured signals are discussed. Section 4 gives a QE comparison of USXRD with silicon XRD. Finally, a summary and future direction is presented in section 5.

2. THE DETECTOR

The detector operating principle is shown schematically in Figure 1a. When photons (with energy E) emitted from a X-ray source, such as a hot plasma, are incident onto a photosensitive cathode, absorption via photoelectric effect creates energetic primary and Auger electrons. A small fraction of the secondary electrons, which are generated by the slowing down of the fast component, is transported to and escapes from the photocathode surface. These photoelectrons are extracted by an applied electric field (~300V to avoid space-charge limitation and reduce tokamak magnetic field effects). Modest energy resolution is achieved by the absorption properties of filters and the intrinsic energy response of the photocathode. The cathode material used here is micromachine finished aluminium, which offers the advantages of well-known QE and availability.

Figure 1b shows a layout of the seven channel USXRD used on ASDEX. The system is built by KMS Fusion, Inc. on a standard 2 3/4" Conflat flange. The major components are: Al cathodes, wire mesh anodes, and filters. A 1mm thick lead filter is used to provide a null reference signal. This is especially important for weak signals. The speed of our detector system is limitd by the amplifier response to 100 µs whereas the photoelectric emission is in $<10^{-17}$s, secondary electron production and transport to cathode surface is in $<10^{-14}$s, and nominal collection time is in $<10^{-12}$s. Fast USXRD system has been built with temporal resolution of less than 50ps for pulsed plasma applications /12/.

The QE of an Al cathode is shown in Figure 2 as the "bare" curve from 10eV to 10keV. The energy response of a filtered channel is the product of the photocathode QE with the transmission of the filter. The sensitivity of filtered diodes for filter thickness of 0.8 µm Al, 0.2 µm C, and 1 µm Be+ 0.7 µm Al are also presented. The bare response is the Los Alamos compilation /13/ for Al_2O_3 (hence the presence of O-K and Al-K edges at 0.5 and 1.4keV, respectively), and the attenuation coefficients for the filters are from Henke, et al. /14/. For the bare channel, the peak QE is 0.2 at 20eV and decreases by two orders of magnitude at 10keV. This QE energy dependence can be understood in terms of a semi-empirical model of Henke, et al. /15/. The predicted QE energy dependence is

$$QE \sim E \cdot \mu(E) \cdot f(E) \qquad (1)$$

where E is the photon energy, $\mu(E)$ is the mass absorption crossection, and $f(E)$ is a slowly varying function of E related to the efficiency of converting the primary electrons into secondaries. At large E, $\mu(E)$ decreases as $1/E^3$, hence leads to decreased QE. In general, the product $\mu(E) \cdot E$ accounts for most of the two orders of magnitude variation in QE. For example for gold and carbon cathodes, $f(E)$ vary by no more than 20% and 30%, respectively, over the above energy range. Moreover, this semi-empirical model accounts for the presence of edges (C-K, O-K and Al-K edges in Figure 2) in QE response. Carbon layers are ever present in vacuum systems.

The detectors were mounted on the outside of the vacuum vessel wall and the distances to the outer edge of the plasmas were 1 m and 0.55 m for D-IIID and ASDEX, respectively. The magnetic fields at the detectors are less than 0.5 kG in both cases. The performances of these detectors can, in principle, be affected by charged and neutral particles, strong magnetic fields and surface coating. Our experiences have been similar to Taylor's /11/, in that particle and magnetic field effects are negligible. Not only did the bare and filtered channels behaved as expected, as will be shown in section 3, the time response of bare channel and H_α-photodiode are nearly perfectly correlated. On the question of surface contamination, we have observed that only the bare USXRD cathode was coated with a thin film, similar to window coating on D-IIID (presumably from glow discharge cleaning), after over 300 plasma discharges. While an absolute calibration has not yet been performed on the "aged" cathodes, we expect that the QE in the VUV region will be affected for the bare channel.

Day, et al. /16/, have shown that a combination of careful photocathode surface preparation, such as micromachined Al cathodes, and storage in vacuum between experiments, have resulted in long term QE stability in the subkilovolt region to better than 15%. However, QE change by ± 200% have also been observed where handling has been more relaxed.

3. EXPERIMENTAL DATA

We present in this section some representative experimental results illustrating the range of applicability of USXRD. Figure 3 shows the waveforms of a 1 MA D-IIID H-mode discharge (53472) with additional heating of 3 MW neutral beam injection (NBI) from 1750 ms to 2200 ms of the discharge. The

initial L-mode phase persited from 1750 ms to 1880 ms as evident by the rise in the H_α signal. During the H-phase (1880 ms - 2220 ms), H_α light is decreased (i.e. reduced edge recycling) while plasma density and soft X-ray radiation (outer Si XRD signal shown here) have increased. An edge localized mode (ELM), occurred at about 2095 ms, resulted in the spike of the H_α signal and decreased electron density and soft X-rays. After the termination of the NBI, the H-phase persisted for another 20 ms before returning to the L-mode. The USXRD signals (2 kHz A/D) are shown in Figure 3 (lower four panels). The "limiter back" diode refers to an unfiltered single channel detector at the back of the 180° pump limiter vacuum duct (see /17/). The limiter has been retracted to about 2 cm in front of the vacuum vessel wall and the front surface is about 3-4 cm from the outer edge of the plasma. This diode has no direct view of the plasma, and only radiation generated by particles interacting with the neutralizer plates or reflected/ scattered VUV light is detected. The remaining three channels view the plasma radially through a 60° mid-plane port. Both unfiltered USXRDs have temporal traces nearly identical to the H_α data. However, the 60° bare channel differs from the H_α in that during the H-phase, the signal rises which is associated with the temperature and density rise during the same period (this diode has response from 10eV - 10keV). For the Al filtered channel, energy response in the range $20eV < E < 60eV$ and $600eV < E < 2keV$, and C filtered channel, energy response in the range $150eV < E < 300eV$ and $600eV < E < 2keV$, the recorded signals are nearly identical to the edge soft X-ray data obtained with the Si XRD. Furthermore, the ELM behavior measured with USXRD is consistent with the H_α and Si XRD data. Thus a single detector system is able to span the useful range from edge plasma (i.e. H_α photodiode) to the hotter emission region (i.e. soft X-ray diode).

A 1.5MA ohmic discharge (53735) on D-IIID is shown in Figure 4 for 0.8 μm Al filtered (peak energy response 30eV and 1.5 keV) and 1 μm Be filtered (peak energy response 1.5keV) USXRDs and a Si XRD. Impurity expulsion started at 1350 ms into the plasma discharge. Followed by sawteeth activities after 1430ms. The waveform of the Be filtered channel and Si diodes are nearly identical. The Al filtered channel showed much reduced fluctuations. This observation is consistent with the conventional interpretation that the sawteeth activities occur in the core plasma, within the q=1 surface, and hence modulating the higher energy photons. In principle, the difference between these filtered USXRD channels should yield the 30eV response, in practice this should be executed with the greatest of care.

A 1MHz transient recorder (WW Scientific Instruments - Signal Memory Recorder) has been used on ASDEX for both H_α photodiode and bare USXRD (VUV) measurements in the upper divertor chamber. Figure 5b shows such a comparison for L-mode discharge (21113) with the following parameters; 320kA plasma current, 3.0×10^{13} cm^{-3} line-averaged electron density and 1MW NBI from 1000ms to 1500ms. The dashed time marker indicates the initial rise in H_α (also the neutral beam injection point) which attained its first peak about 20ms later, the solid marker. Highly correlated signals between the H_α and the VUV are shown in Figure 5a in magnified time scale for the same discharge. The interesting point to be made here is that the initiation points for each peak are nearly identical, see the time markers in Figure 5a, with the VUV signals having both broader peaks and longer decay time constants. The edge oscillation period is 32.64ms with 5ms lag of the VUV peaks relative to the corresponding H_α peaks. Finally, the disruption phase of the same discharge is presented in Figure 5c. The initial H_α-spike corresponds to a broad VUV feature which peaked 3.36ms later. The subsequent H_α are very large, while the corresponding VUV signals are extremely small.

The broader VUV response relative to the H_α spikes is most likely related to some plasma equilibration time within the divertor chambers. The USXRDs have demonstrated temporal resolution of better than 200µs on D-IIID ELMs.

4. DIODE COMPARISON

In this section we examine the range of the applicability of the Si XRD and USXRD detectors. The sensitivities of these detectors are plotted in Figure 6. The heavy solid curve is the response of micromachined Al cathode. The curve with symbol "1" is the NBS transfer standard USXRD with deposited Al cathode (calibration from 10eV - 250eV) /18/. The difference between these two types of cathodes is small, less than ±20%. The curve Si diode/250 gives the quantum efficiency of the Si XRD divided by 250 for the purpose of presentation. The small response at 100eV is the result of Si $L_{II\ III}$ absorption edge. We modelled the Si diode as 1µm Be window, 0.5µm Si deadlayer and 200µm Si wafer. In the 3keV - 10keV range (FWHM of Si QE), the QE of the Si diode is over 3500 times that of the Al photocathode. However, for high temperature plasmas, T_e > 1keV, this difference is surmountable with good preamplifiers (see Figure 4). Whereas

the USXRD is gain or amplifier limited in this energy range, the Si XRD is shot noise limited, at low photon flux.

QE enhancement has been found for certain alkali halides, iodines and semiconductors in the ultrasoft X-ray range. A comparison of CsI with Al cathode is shown in Figure 6. Over most of the range, enhanced photoemission by a factor of 30 is obtained. This is generally attributed to the increased scattering length for secondary electrons below the Fermi level, thus allowing more electrons to reach the cathode surface for extraction. On the negative side, however, the response of CsI photocathodes is known to degrade in air with 20% to 25% humidity for more than a few hours, and a slower component of the photoemission process, a few percent level of the main component seems to persist for about 100 ps /19/.

Finally, we estimate the range of plasma temperature for which these detectors will be useful. Figure 7 gives the calculated response of USXRD with different filters. The radiation is assumed to be pure Bremsstrahlung and the signal normalized to the bare XRD channel as follows:

$$\text{Ratio} = \int_{10eV}^{100keV} e^{-E/Te}\, T(E)QE(E)dE \Big/ \int_{10eV}^{100keV} e^{-E/Te}\, QE(E)\, dE, \qquad (2)$$

here E, T_e, T(E) and QE(E)are the photon energy, electron temperature, filter transmission and quantum efficiency, respectively. The detection limit defined here is to serve as a rough estimate based on reasonable time response (1ms) for 10^{10} V/A signal gain. Strong line radiations can certainly enhance the detected signals, and thus these curves should serve as a lower bound. For example, the ratios of the USXRD signals, in Figure 3 main plasma, yields 100 for Al/bare and 150 for C/bare. While the Al channel is close to the estimate, the C channel is about 70 times better than the Bremsstrahlung model. This decrepancy is the result of strong line radiation in the 100eV - 300eV range.

5. SUMMARY AND FUTURE DIRECTIONS

The ultrasoft X-ray diodes on D-IIID and ASDEX have proven to be valuable VUV and soft X-ray diagnostics. These simple and compact detectors have served to bridge the photon energy gap between the H_α photodiodes and Si XRDs. While the QE of USXRDs are about 3500 less than that of Si diodes (energy range 3keV to

10keV), for hot plasma, T_e > 1keV, sawteeth activities are clearly observed.

For future application, the question of toroidal asymmetry, divertor plasma radiation, edge recycling and pump limiter neutralizer plates emission can be addressed with USXRDs. Better energy resolution with simple combinations of filter plus reflection on multilayer mirror techniques should give resolving power in the range $E/\Delta E$~5-20. Spatial imaging USXRD arrays can compliment the present Si XRD arrays for the edge plasma. Furthermore, we feel that temporal resolution of better than 0.1 μs will be useful for charge balance and recycling activity studies.

The QE of many photocathodes has been measured (particularly aluminium) and thus absolute measurements are possible. The effects of magnetic fields on the total detected photocurrent can, in principle, alter the QE and temporal responses. While we feel these effects can be minimized by higher bias voltage (>1000 V), smaller anode to cathode gap (< 1 mm) and anode housing around the cathode, the magnetic field effects should be investigated in greater depth.

ACKNOWLEDGEMENT

One of us, P. Lee, is indebted to H. Oona for the initial help on this project. Furthermore, P. Lee and J. Gernhardt have benefitted from many useful discussions with S. von Goeler on the solid state XRDs. Finally we would like to thank D.E. Roberts for helpful suggestions regarding this manuscript.

Figure captions

Figure 1. (a) The detector operating principle is based on measurements of photoelectric current generated by the VUV and soft X-ray photons. Modest energy resolution is obtained by the transmittance of the filter and the quantum efficiency of the photocathode.

(b) Schematic of a USXRD based on a 2 3/4" Conflat flange.

Figure 2. QE of aluminium photocathode based on LANL compilation /13/. The edges at 280eV, 500eV and 1.4keV are the C-K, O-K and Al-K absorption edges, respectively. The net efficiencies of filtered diodes are shown as broken lines.

Figure 3. Waveforms for a H-mode discharge on D-IIID. The USXRD signals are shown on the lower four panels.

Figure 4. Ohmic plasma on D-IIID with sawteeth activity initiated at 1430ms into the discharge, the 1 μm Be filtered channel with response around 1.5keV exhibited sawteeth nearly identical to the Si XRD. The edge channel, 0.8 μm Al, shows much less activity.

Figure 5. ASDEX L-mode discharge with NBI from 100ms to 1500ms. Data measured with 1MHz transient recorder in the upper divertor chamber. Bare USXRD is compared with H_α photodiode. (a) early NBI phase, (b) ohmic to disruption, and (c) disruption phase.

Figure 6. Comparison of photocathode and Si diode QE responses. Photocathodes shown are micromachined Al (heavy solid), vacuum deposited Al (NBS "1"), and CsI ("+"). The Si diode response has been divided by 250 (thin solid). The small peak around 100eV is due to the $L_{II,III}$ of Si.

Figure 7. Ratio of filtered to bare USXRD responses as a function of Bremsstrahlung temperature. Since line radiation has not been accounted for, these curves should serve as a lower bound.

References

/1/ S. von Goeler, W. Stodiek and N. Sauthoff, Phys. Rev. Lett. 33, 1201 (1974).

/2/ N. Sauthoff, S. von Goeler and W. Stodiek, Nucl. Fusion 18, 1445 (1978).

/3/ G.L. Jahns, et al., Nucl. Fusion 22, 1049 (1982).

/4/ R.S. Granetz, A.W. Edwards, R.D. Gill and A. Weller, Proc. 14th Eur. Conf. Contr. Fusion Plasma Phys., 1256 (Madrid 1987).

/5/ M. Kornherr, et al., Proc. 13th Eur. Conf. Contr. Fusion Plasma Phys., 84 (Schliersee 1986).

/6/ see for example, "Physics of Plasma-Wall Interaction in Controlled Fusion", Eds. D.E. Post and R. Behrisch, NATO ASI, Vol. 131, Plenum Press, N.Y. (1984).

/7/ F. Wagner, M. Keilhacker, et al., J. Nucl. Mater. 121, 103 (1984).

/8/ R.H. Day, in AIP Conf. Proc. 75, Eds. D.T. Attwood and B.L. Henke (Am. Inst. of Phys., N.Y.) p. 44 (1981).

/9/ V.W. Slivinski and H.N. Kornblum, Rev. Sci. Instrum. 49, 1204 (1978), R.H. Day, P. Lee, E.B. Saloman, and D.J. Nagel, Los Alamos Report, LA-7941-MS (1981).

/10/ A large body of neutron effects on USXRDs exists but is seldom existent in the open literature. The main damages are to preamplifiers and signal cables.

/11/ S.J. Zweben, C.R. Menyuk, and R.J. Taylor, Rev. Sci. Instrum. 50, 972 (1979).

/12/ see ref. 8, figure 3.

/13/ R. Hockaday, private communication (1986).

/14/ B.L. Henke, P. Lee, T.J. Tanaka, R.L. Shimabukuro and B.K. Fujikawa, At. DATA, Nucl. DATA Tables 27, 1 (1982).

/15/ B.L. Henke, J.A. Smith and D.T. Attwood, J. Appl. Phys. 48, 1852 (1977).

/16/ R.H. Day, P. Lee, E.B. Salmon, and D.J. Nagel, J. Appl. Phys. 52, 6965 (1981).

/17/ a layout of the pump limiter is given in: M.A. Mahdavi, et al., J. Nucl. Mater. 128/129, 468 (1984).

/18/ L.R. Canfield, R.G. Johnson and R.P.Madden, Applied Optics 12, 1611 (1973); E.B. Salomon and D.L.. Ederer, Applied Optics 14, 1029 (1975).

/19/ see ref. 8.

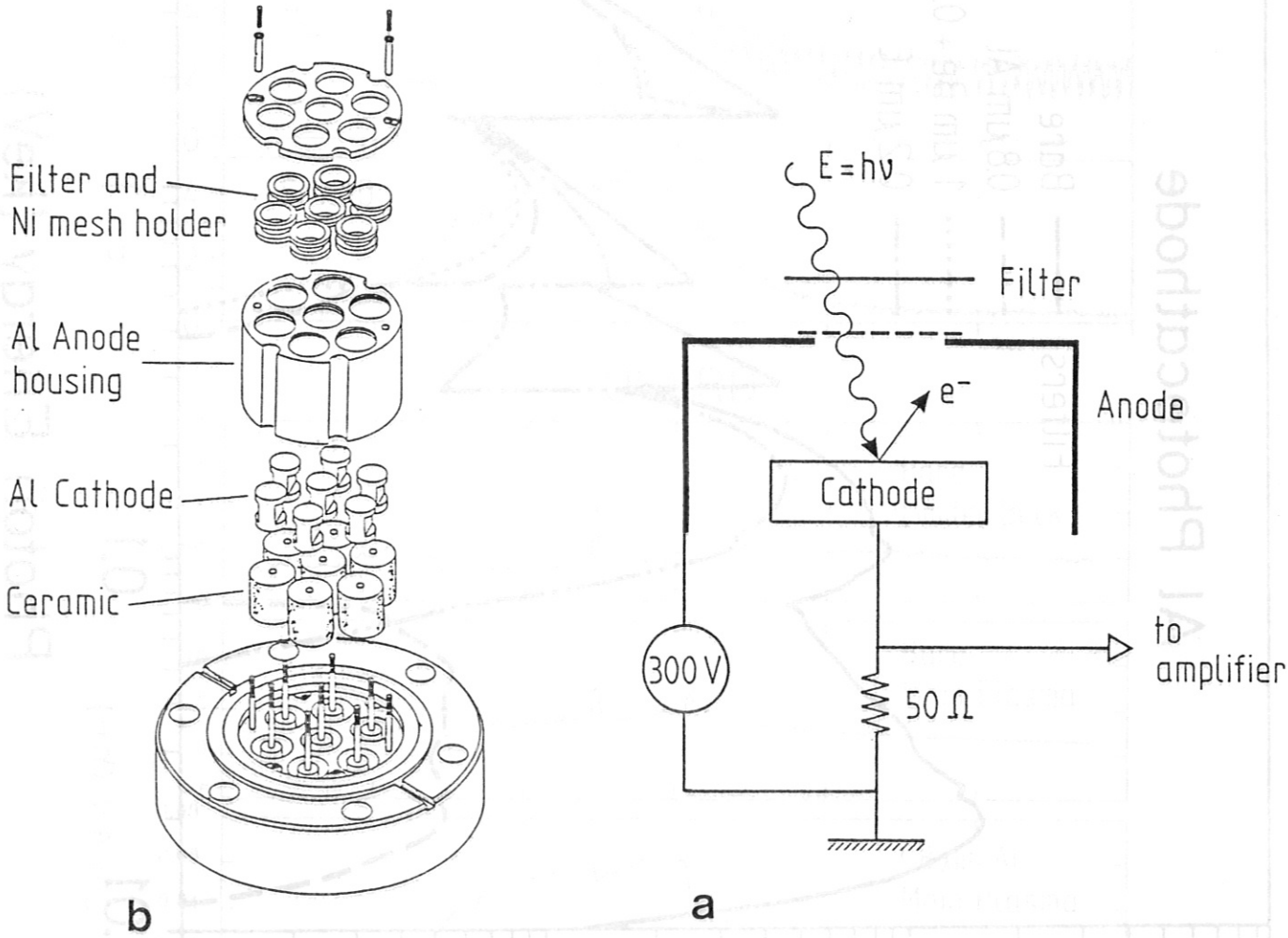
Filter and
Ni mesh holder
Al Anode
housing
Al Cathode
Ceramic
b
E = hν
Filter
e⁻
Anode
Cathode
300 V
50 Ω
to
amplifier
a

Fig. 1

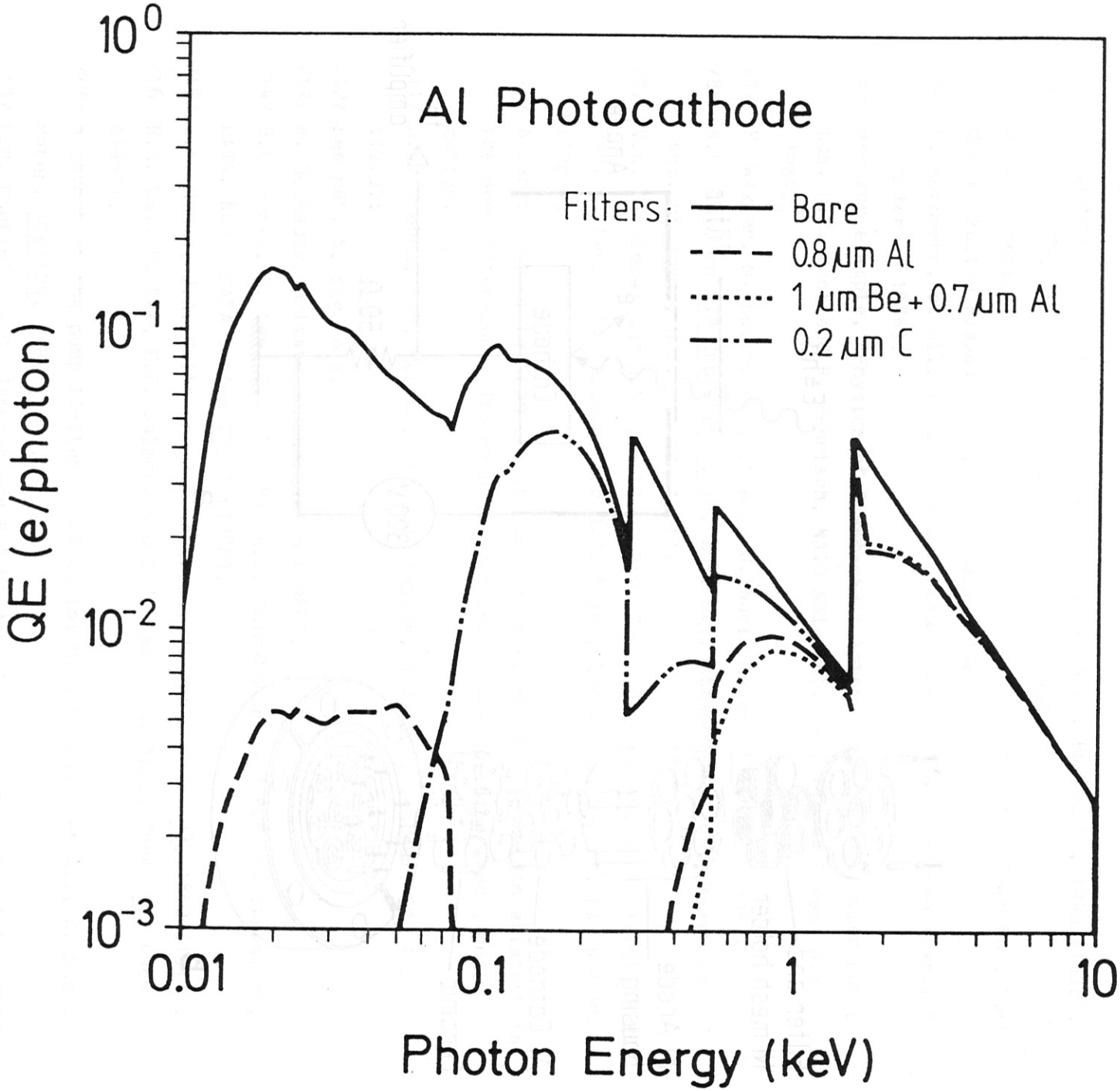
Al Photocathode
Filters:
Bare
0.8 μm Al
1 μm Be + 0.7 μm Al
0.2 μm C
QE (e/photon)
10^0
10^{-1}
10^{-2}
10^{-3}
0.01
0.1
1
10
Photon Energy (keV)

Fig. 2

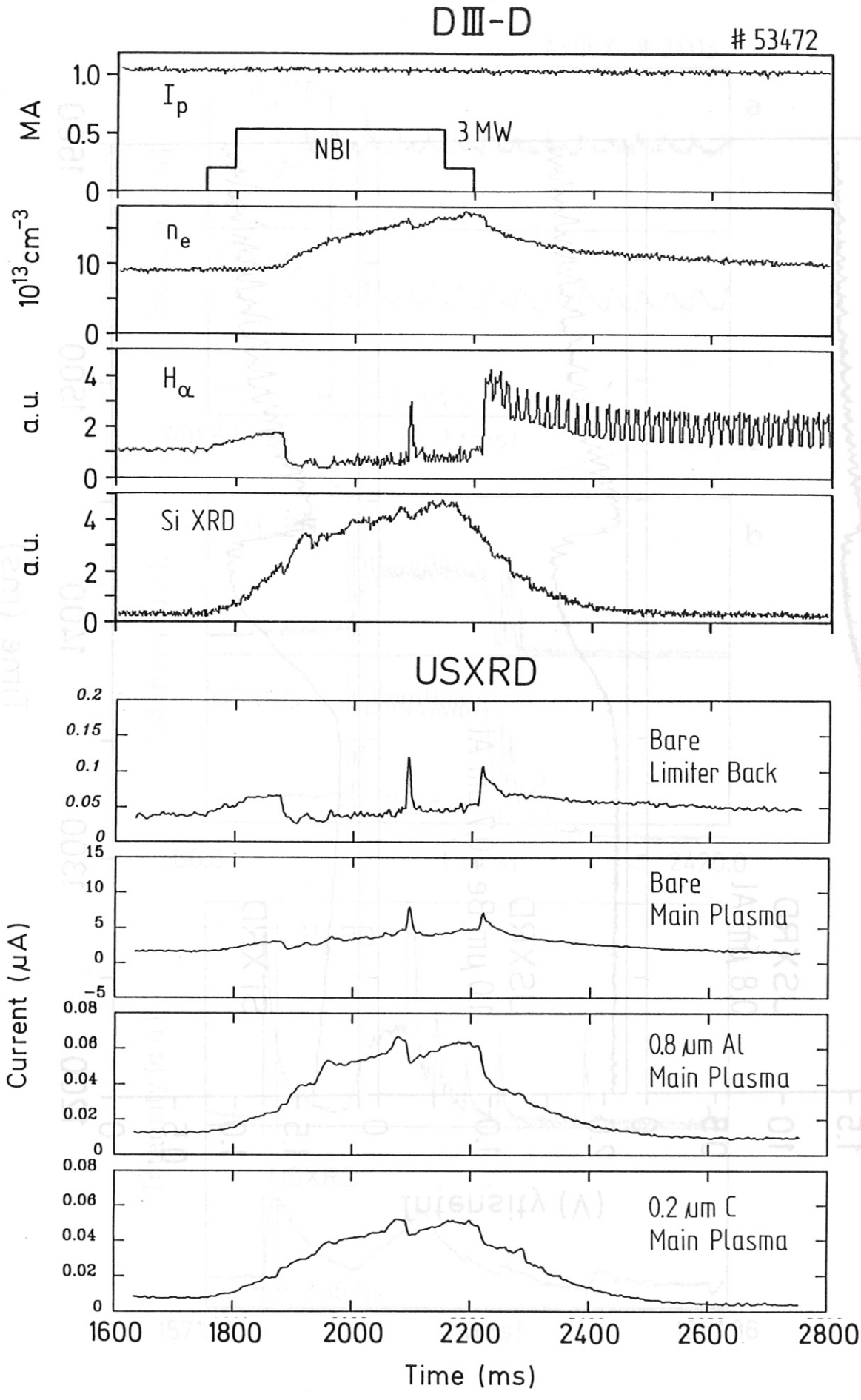
DIII-D
53472
1.0
0.5
0
MA
I_p
NBI
3 MW
$10^{13}cm^{-3}$
n_e
10
0
a.u.
H_α
4
2
0
Si XRD
USXRD
0.2
0.15
0.1
0.05
Bare
Limiter Back
15
10
5
−5
Bare
Main Plasma
Current (μA)
0.08
0.06
0.04
0.02
0.8 μm Al
Main Plasma
0.2 μm C
Main Plasma
1600
1800
2000
2200
2400
2600
2800
Time (ms)

Fig. 3

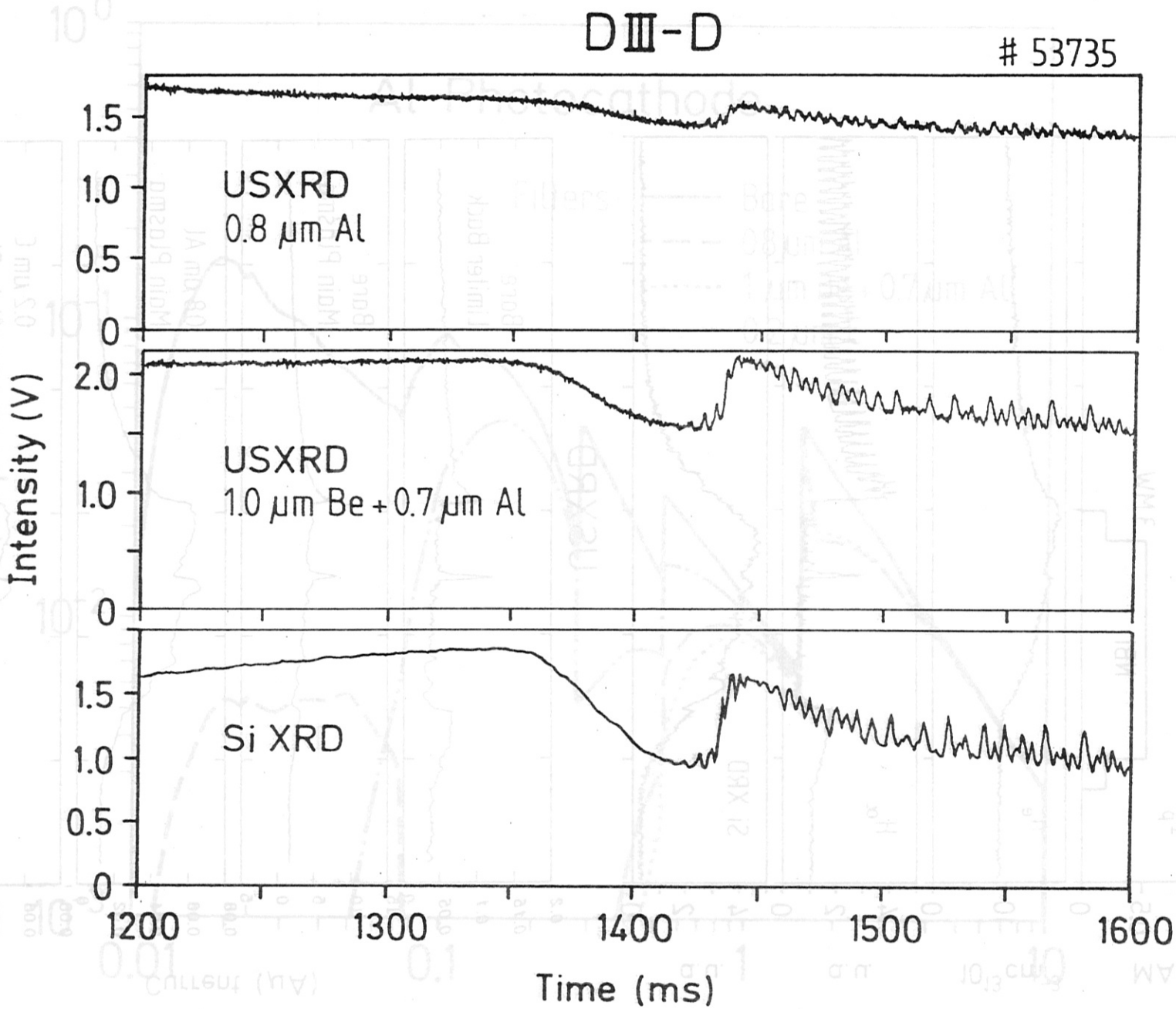
DIII-D
53735
USXRD
0.8 μm Al
USXRD
1.0 μm Be + 0.7 μm Al
Si XRD
Intensity (V)
Time (ms)
1200
1300
1400
1500
1600

Fig. 4

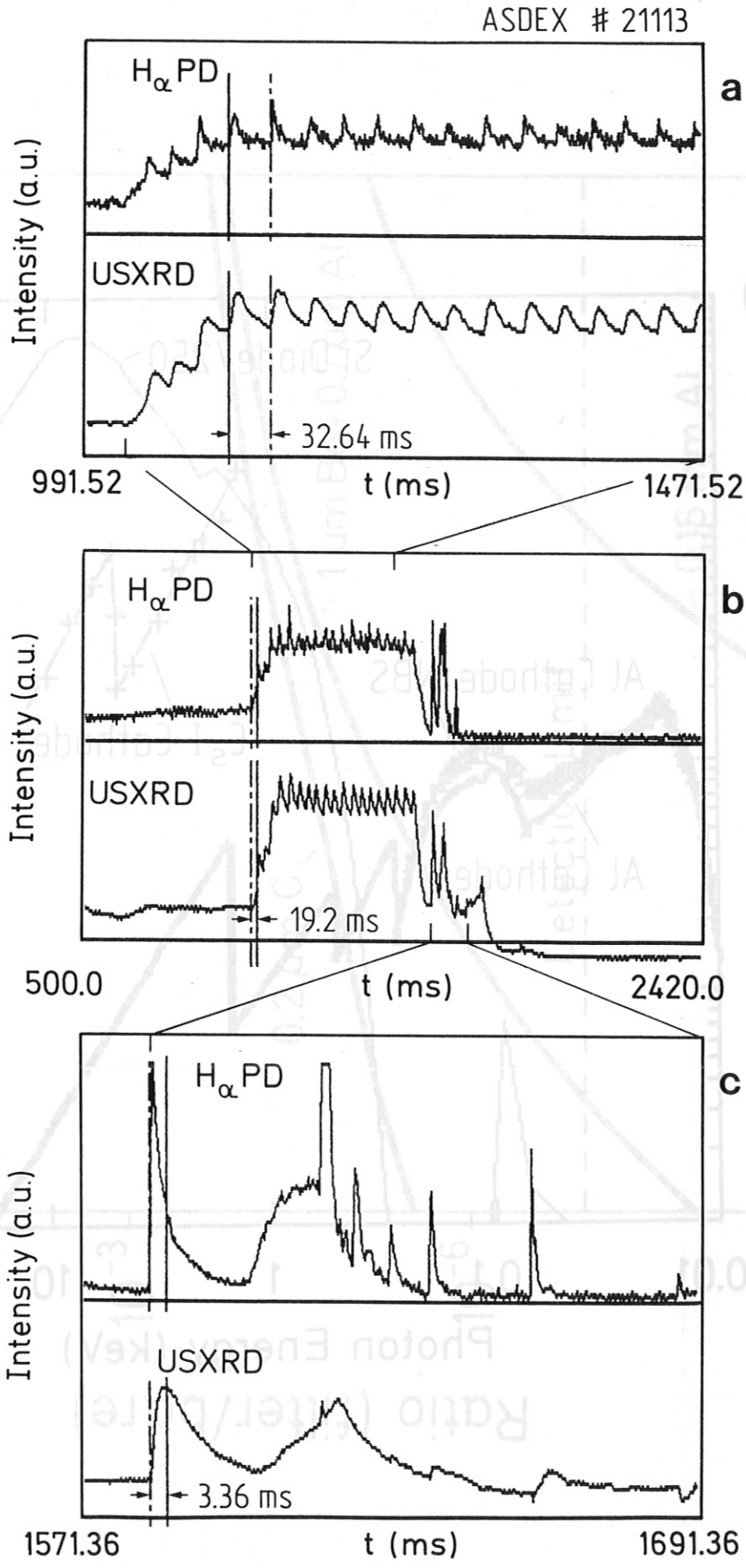
ASDEX # 21113
H_α PD
a
USXRD
Intensity (a.u.)
32.64 ms
991.52
t (ms)
1471.52
H_α PD
b
USXRD
Intensity (a.u.)
19.2 ms
500.0
t (ms)
2420.0
H_α PD
c
USXRD
Intensity (a.u.)
3.36 ms
1571.36
t (ms)
1691.36

Fig. 5

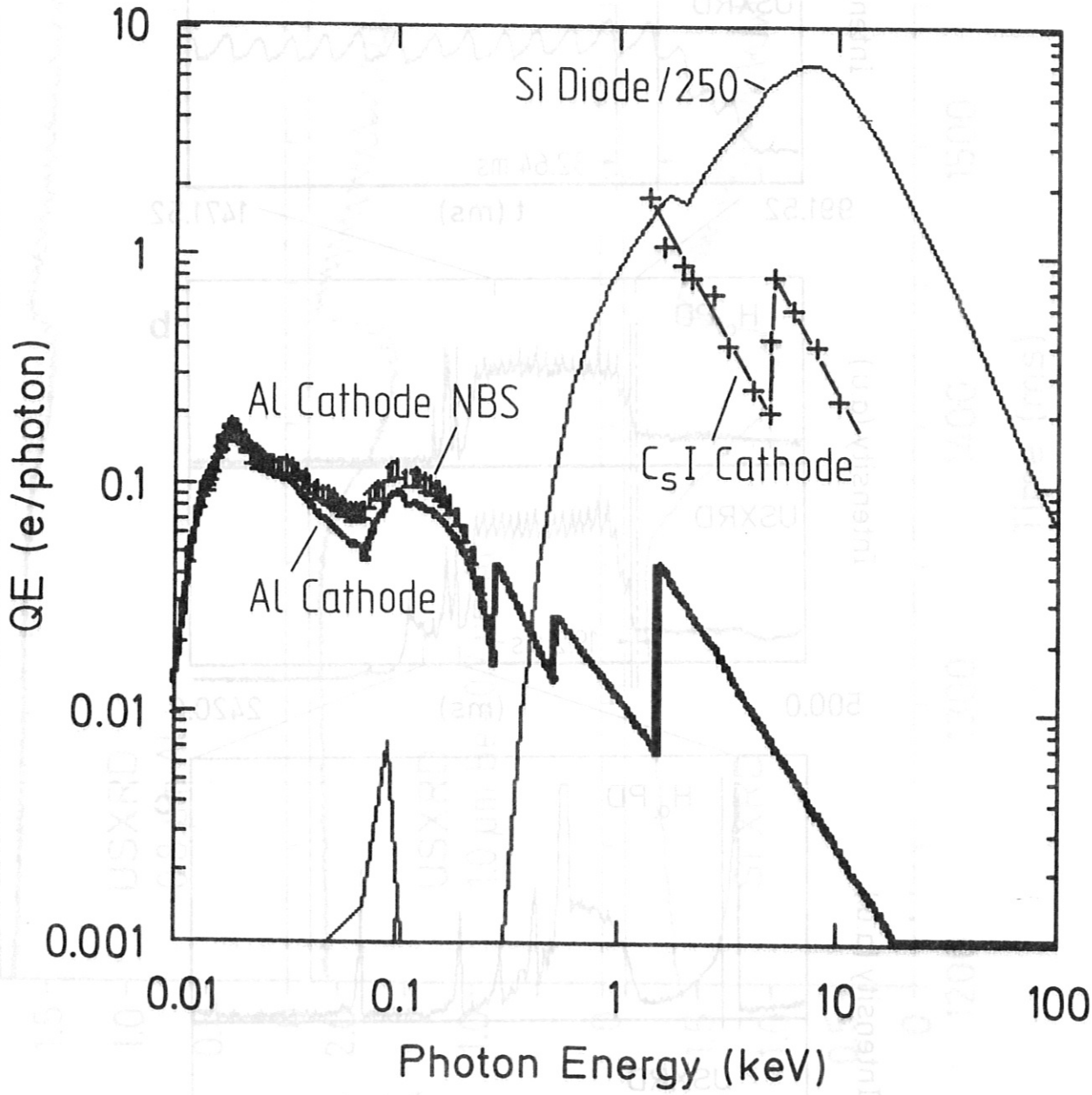
10
1
0.1
0.01
0.001
QE (e/photon)
Si Diode/250
Al Cathode NBS
Al Cathode
C_sI Cathode
0.01
0.1
1
10
100
Photon Energy (keV)

Fig. 6

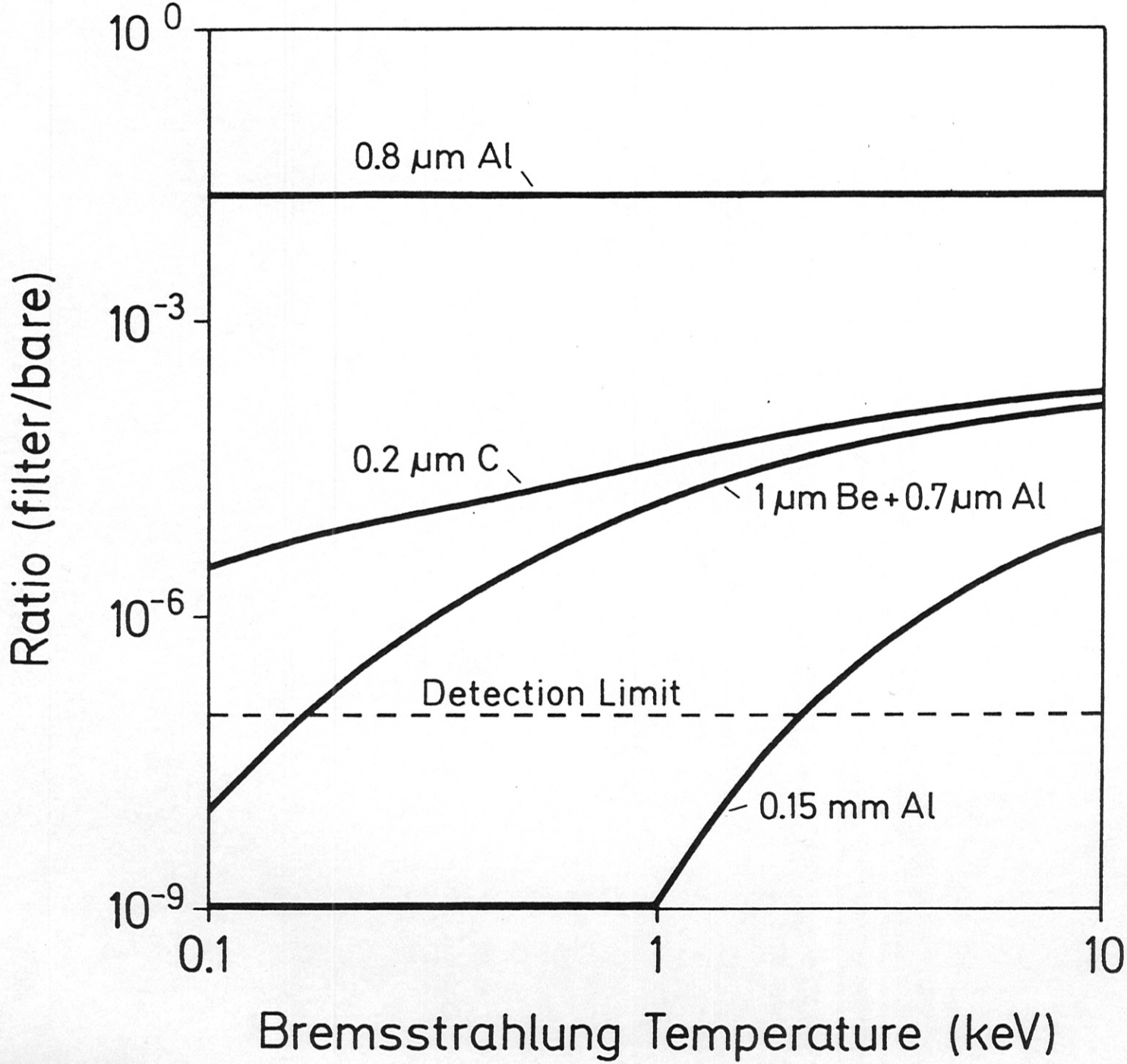
10 0
10-3
10-6
10-9
Ratio (filter/bare)
0.8 μm Al
0.2 μm C
1 μm Be + 0.7 μm Al
Detection Limit
0.15 mm Al
0.1
1
10
Bremsstrahlung Temperature (keV)

Fig. 7